Full Length Article

Effects of Nd/Gd value on the microstructures and mechanical properties of Mg–Gd–Y–Nd–Zr alloys

Xuan Liu, Zhiqiang Zhang, Qichi Le *, Lei Bao

Key Lab of Electromagnetic Processing of Materials, Ministry of Education, Northeastern University, 314Mailbox, Shenyang 1100819, China

Abstract

Four Mg–Gd–Y–Nd–Zr alloys were prepared by mold casting to investigate the effects of Nd/Gd ratios on microstructures and mechanical properties. The as-cast alloys mainly consist of α-Mg and β-Mg_5(GdYNd). Volume fractions of the second phase increase and grains were slightly refined with the rising Nd/Gd ratio, when the alloying addition is equal. Meanwhile, fibers of second phase also increase in the extruded alloys when the Nd/Gd value increases. However, the Nd/Gd ratio could hardly influence the mechanical properties of the extruded alloys. The aging hardening response of the extruded alloy differs due to different Nd/Gd ratios. The potential mechanisms have also been discussed in detail.
© 2016 Production and hosting by Elsevier B.V. on behalf of Chongqing University. This is an open access article under the CC BY-NC-ND license (http://creativecommons.org/licenses/by-nc-nd/4.0/).

Keywords: Mg–Gd–Y–Nd–Zr alloy; Microstructure; Inverted extrusion; Heat treatment; Mechanical properties

1. Introduction

Magnesium alloys are the lightest structural materials, known for their high specific strength, specific stiffness and good cast-ability [1]. However, their poor performance on strength, particularly at elevated temperatures, restricts the application of Mg alloys [2].

Mg alloys with good heat-resistance as well as high strength have been a spot for study. Some kinds of heat-resistant magnesium alloys have been successfully applied in the automobile and aerospace industries, taking Mg–Al–RE, Mg–Al–Ca and Mg–RE series for examples [3–5], while Mg–RE alloys are the most important heat-resistant magnesium alloys, capable of maintaining a certain extent of strength at the temperature about 200 °C ~ 300 °C [6–8]. The heavy rare earth elements (Gd and Dy, etc.) significantly improved the aging hardening response of Mg alloys, when the addition is over 10 wt.% [9]. Thus, Mg–Gd based alloys with large addition of Gd have been extensively studied in order to develop more splendid magnesium alloys with high strength and good heat-resistance. It is covered that alloy Mg–17Gd–0.51Zr with extrusion and T5 heat treatment has excellent mechanical properties (an ultimate tensile stress of 400 MPa) [10].

However, on consideration of the cost, the most typical Mg–Gd based alloys should be Mg–Gd–Y–Zr alloys, especially Mg–10Gd–3Y–0.6Zr (wt-%). A mass of research developed on the basis of the Mg–10Gd–3Y–0.6Zr showed outstanding properties as well [10–14]. Moreover, light rare earth elements like Nd and Pr have been added to enhance the properties of Mg–Gd–Y–Zr alloys. The effect of Nd addition on the microstructure and mechanical properties of Mg–8Gd–5Y–2Zn–0.5Zr (wt-%) has been studied [15]. The role of each rare earth element in magnesium differs from each other. Adjusting the content of each rare earth element should be the primary method in a large number of studies, on the premise that the total addition of RE element was controlled in a scale of certain extent.

Currently, research concerning the effect of Nd/Gd values on the microstructure and mechanical properties is not widely developed. In this work, four Mg–Gd–Y–Nd–Zr alloys with different Nd/Gd values were prepared. The effects of Nd/Gd value on the microstructures and mechanical properties of the as-cast and extruded Mg–Gd–Y–Nd–Zr alloys were investigated.

---

* Corresponding author. Key Lab of Electromagnetic Processing of Materials, Ministry of Education, Northeastern University, 314Mailbox, Shenyang 1100819, China. Tel.: +86 24 83683312; fax: +86 24 83681758.
E-mail address: qichil@mail.neu.edu.cn (Q. Le).

2. Experimental

High purity elemental Mg (>99.95%), Mg–25Gd (wt.%), Mg–50Y (wt.%), Mg–25Nd (wt.%) and Mg–30Zr (wt.%) were prepared as the raw material. The alloys were melted in a mild steel crucible, heated by an electric resistance furnace. Flux was also used to purify the melt, as well as prevent it from burning. The melted alloys were homogenized at about 710 °C for 10 min. Then, the melt was poured into a preheated steel mold with a diameter of 60 mm. The compositions of the alloys were obtained by chemical analysis (an inductively coupled plasma mass spectrometry), listed in Table 1. Homogenization treatment was carried out at 510 °C for 16 h. After homogenization, the ingots were extruded reversely into rods with a diameter of 12 mm at the temperature of 400 °C. The extrusion ratio was 15:1. Aging after extrusion was implemented at 200 °C. Then the rods were machined into tensile specimens of 6 mm gauge diameter and 25 mm gauge length, according to the ASTM standard B557M-10. Tensile test was performed by universal tensile testing machine (the speed of tensile was 1 mm/min) at room temperature (RT) and elevated temperature, and the alloys took 10 min to balance the temperature before tensile test at elevated temperatures.

Table 1
Chemical compositions of investigated alloys (wt-%).

Alloys	Nominal composition	Gd	Y	Nd	Zr	Fe	Mg
1	Mg–8Gd–3Y–2Nd–0.6Zr	7.09	2.96	2.06	0.42	0.035	Bal
2	Mg–10Gd–3Y–4Nd–0.6Zr	9.49	3.06	3.84	0.286	0.021	Bal
3	Mg–6Gd–3Y–4Nd–0.6Zr	5.26	3.86	4.33	0.330	0.010	Bal
4	Mg–8Gd–3Y–6Nd–0.6Zr	7.82	3.19	5.89	0.303	0.017	Bal

Microstructures were observed by optical microscope (OM) and scanning electron microscope (SEM) coupled with an energy dispersive X-ray analyzer (EDX). The phase analysis was performed with an X-ray diffractometer (XRD). Linear intercept method was applied to determine the grain size of the alloys.

3. Results and discussion

3.1. Microstructures of the as-cast alloys

Microstructures of the as-cast alloys are shown in Fig. 1. Similar to the typical microstructures of Mg–Gd–Y–Zr alloys, microstructures of the investigated Mg–Gd–Y–Nd–Zr alloys are mainly made up of nearly equiaxed grains and discontinuous second phases around grain boundaries. It is worth mentioning that Alloy 1 and Alloy 3 have the same amount of RE element. However, the area fraction of second phase in Alloy 1 is about 17.6%, which is lower than that in Alloy 3 (21.7%). This is also similar to the case of Alloy 2 (27.3%) and Alloy 4 (31.7%). Then it could be seen that the second phase increases as the Nd/Gd values grow up, keeping the RE addition the same.

According to the binary phase diagrams of Mg–Gd, Mg–Y and Mg–Nd [16], the ultimate solid solubilities of Gd, Y and Nd in Mg are 23.3 wt.%, 12 wt.% and 3.6 wt.%, respectively. Meanwhile, the solubility of all the three element decreases as the temperature goes down. Thus, it is more possible that Nd would likely segregate around the grain boundaries due to the limited equilibrium solid solubility. Thus, it is accessible that the second phase would increase rapidly as Nd/Gd value rises up. Although some slight grain refining effects (from ~25 μm to
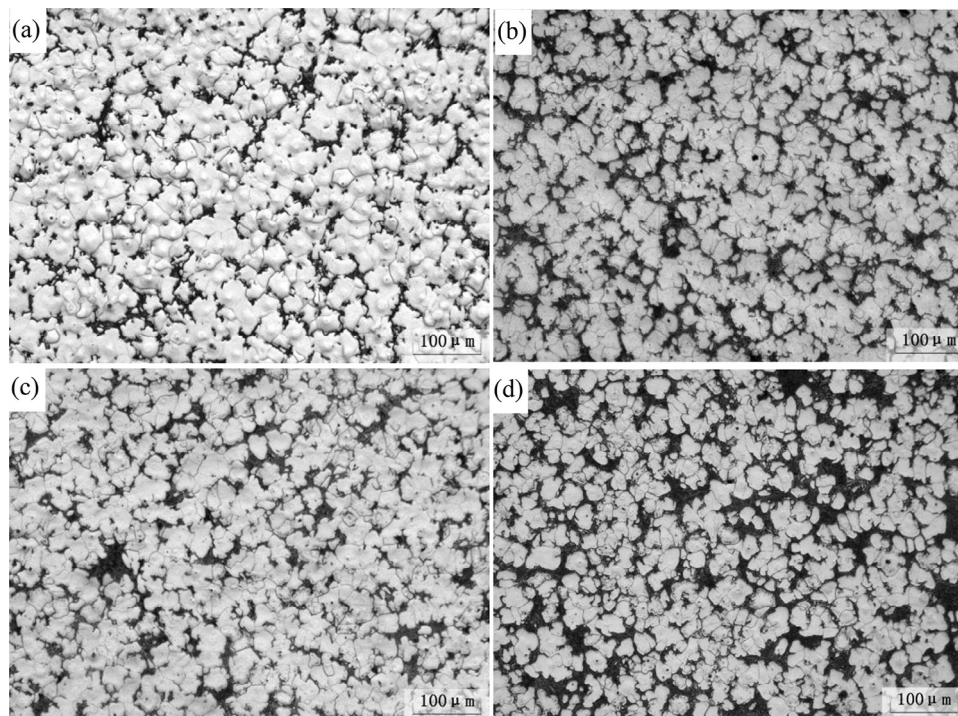

Fig. 1. Optical microstructures of the as-cast alloys. (a) Alloy 1: Nd/Gd = 0.25; (b) Alloy 2: Nd/Gd = 0.4; (c) Alloy 3: Nd/Gd = 0.67; (d) Alloy 4: Nd/Gd = 0.75.
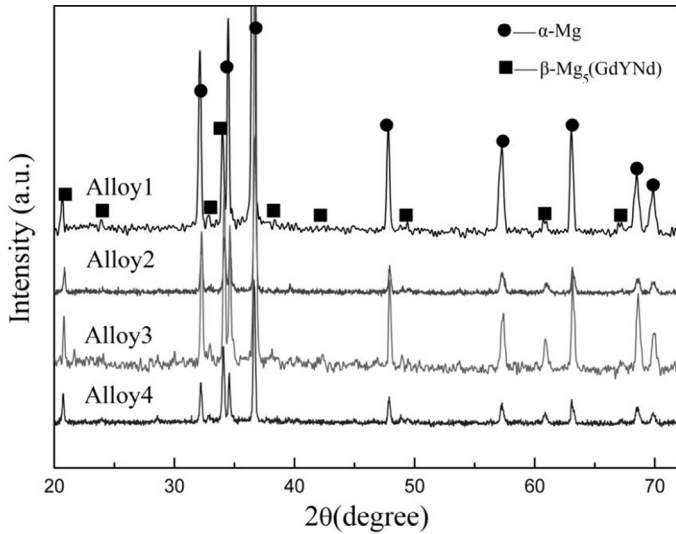
Fig. 2. XRD patterns of the as-cast alloys.

Fig. 3. SEM image of Alloy 4.

~19 μm) could be observed when adding more RE to the alloys, the grain sizes of the as-cast alloys are not much influenced by the Nd/Gd ratios, which has also been reported in our published work [17]. It has been reported that Gd and Nd addition has grain refining effects on Mg alloys by inhibiting the migration of grain boundaries [18,19]. However, Gd and Nd might have close grain refining effects. Thus, the grain size always remains close by replacing part of Gd with Nd when keeping the total alloying amount the same.

The phase compositions of the as-cast alloys by XRD analysis are shown in Fig. 2. It indicates that all of the four as-cast alloys mainly consist of α-Mg solid solution and β-Mg_5(GdYNd) compound. It has been reported in Mg–Gd–Y alloys that rare earth elements blend with each other, forming $Mg_5(Gd_{1-x}Y_y)$ compound [20], which should be ascribed to the similitude of the rare earth element. The compound in this work should be similar to that. It could be seen that the Nd/Gd ratios could not affect the phase compositions according to the XRD patterns. However, they might be able to change the specific element content in the β-Mg_5(GdYNd) compounds. Meanwhile, due to the non-equilibrium solidification, the morphology of the second phase should be pseudo-eutectics, as shown in Fig. 3.

3.2. Microstructures of the extruded alloys

Fig. 4 shows the optical microstructures of the extruded alloys. The second phase was broken and elongated throughout the longitudinal section, paralleling the direction of extrusion. Fig. 5 shows the SEM image and corresponding EDS result of as-extruded alloy. It proves that these elongated phases are rich in RE element. The EDS result of point 1 (Fig. 5b) further indicates that their chemical composition is Mg-4.94 at.% Gd-2.43 at.% Y-5.41 at.% Nd, which refers to β-Mg_5(GdYNd). It is quite possible that these crushed second phases derived from the residual phase during the high temperature homogenization treatment.
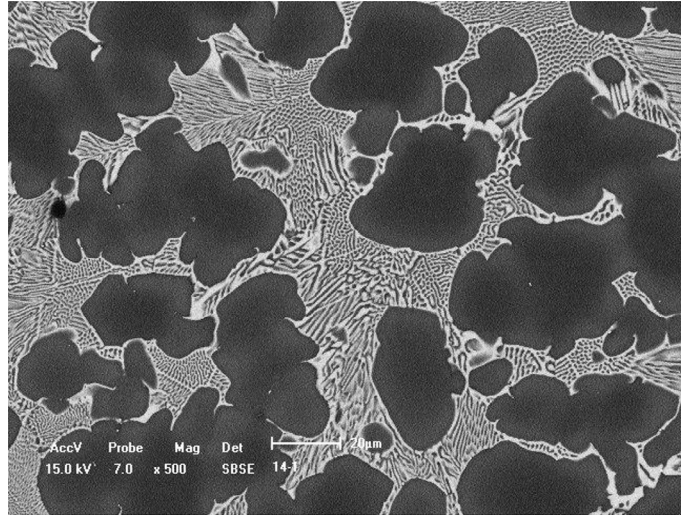
It could be clearly seen that dynamic recrystallization (DRX) is observed in the extruded alloys, as shown in Fig. 4b. As the deformation temperature is 400 °C, slip becomes the main plastic deformation mechanism, and the migration of the grain boundaries is fully promoted. Due to the inhibition of the residual second phases mentioned above, the density of the dislocations is enlarged rapidly, as well as the lattice distortion, and the dislocations would pile up around the interphases between the second phases and the grain boundaries. Subsequently, subboundaries and dislocation cells are easy to be formed. After that, the subboundaries could absorb the dislocations to increase the misorientation among them, forming the high-angle boundaries. On the other hand, RE element could decrease the stack-fault energy, promoting the process of DRX. Finally, the movement of the high-angle boundaries eliminates the subboundaries, and DRX is achieved. However, the precipitations could also prevent the migration of the recrystallized grain boundaries. The grains are clearly larger than those around where the precipitations stay, as shown in Fig. 4b and d.

There are two forms for the crushed second phase: one is a fiber-like form, distributing like bamboo joint, the other is a tiny particle-like form, spreading intensively. The Nd/Gd ratios could obviously affect the microstructures of as-extruded alloys. For alloy 1, whose Nd/Gd ratio is 0.25 (2:8), the crushed second phases are mainly composed of tiny particle-like form, as shown in Fig. 4a. However, when the Nd/Gd ratio is 0.67 (4:6), it could be seen that the fiber-like second phase increases rapidly, as shown in Fig. 4e.

With the Nd/Gd value growing up, the size of the residual precipitations is increasing. It is reasonable that the solid solubility of Nd in Mg is smaller than that of Gd. The drive force to solve Nd in to the matrix is less than that to solve Gd into the matrix. After homogenization, size of the remaining precipitations in alloys with the large Nd/Gd values is much larger than those in alloys with small Nd/Gd values. As a consequence, it can be concluded that content of the polygonal precipitations in
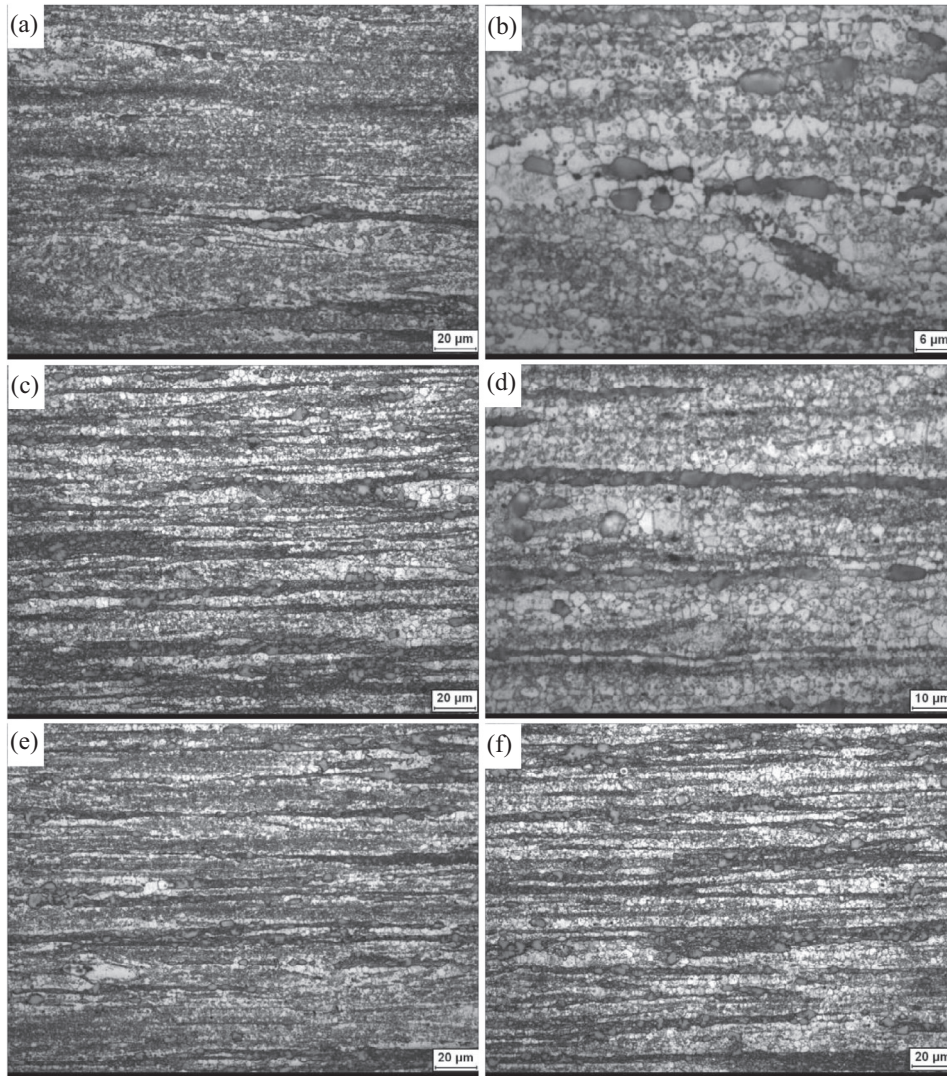
Fig. 4. Optical Microstructures of the extruded alloys. (a and b) Alloy 1; (c and d) Alloy 2; (e) Alloy 3; (f) Alloy 4.

the extruded alloys tend to be increasing as the Nd/Gd value of the alloy ascends.

3.3. Mechanical properties

The tensile properties at room temperature of the three alloys are summarized in Table 2. The Nd/Gd ratios would not much influence the mechanical properties of the as-extruded alloys, when keeping the alloying addition same. The ultimate tensile strength (UTS) and tensile yield strength (TYS) of Alloy 1 (Nd/Gd = 0.25) are 315 MPa and 271 MPa, respectively, while those of Alloy 3 (Nd/Gd = 0.67) are 315 MPa and 298 MPa, respectively. It could be seen that the mechanical properties of
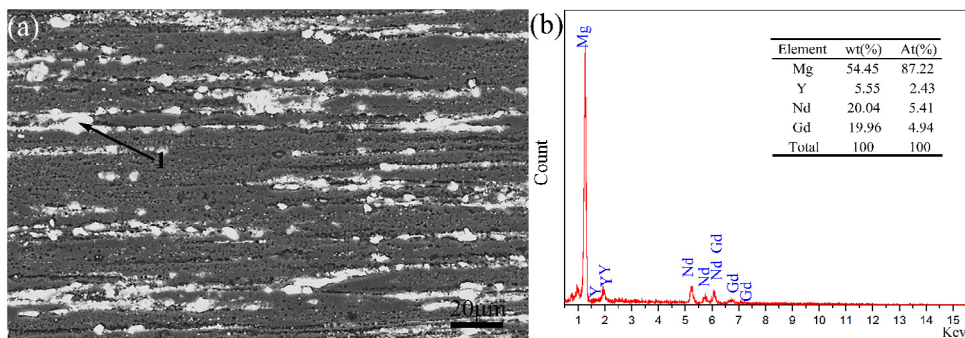

Element	wt(%)	At(%)
Mg	54.45	87.22
Y	5.55	2.43
Nd	20.04	5.41
Gd	19.96	4.94
Total	100	100

Fig. 5. (a) SEM image of the extruded Alloy 4; (b) EDS result of point 1 in (a).

Table 2
Mechanical properties of the alloys at room temperature.

Properties	Alloys							
	Alloy 1		Alloy 2		Alloy 3		Alloy 4	
	Ext	Ext-T5	Ext	Ext-T5	Ext	Ext-T5	Ext	Ext-T5
UTS(MPa)	315 ± 6	358 ± 3.1	340 ± 6.2	379 ± 2.3	315 ± 5.5	354 ± 2.8	338 ± 8.9	365 ± 4.5
TYS(MPa)	271 ± 7.5	282 ± 2.0	300 ± 6.7	332 ± 1.9	286 ± 4.7	298 ± 4.6	291 ± 3.4	308 ± 2.1
ε(%)	11.3 ± 2.3	2.6 ± 0.5	1.6 ± 0.3	0.8 ± 0.2	2.6 ± 0.9	2.1 ± 0.6	2.4 ± 0.8	1.6 ± 0.4

Note: Ext: extruded; T5: peak-aged at 200 °C.

Alloy 1 and 3 are almost the same, except for the elongations, as listed in Table 2. Alloy 1 has the largest elongation of 11.3%, but Alloy 3 shows a poor elongation of 2.6%. It suggests that the increasing Nd/Gd ratio seriously deteriorates the elongations. It is similar for Alloys 2 and 4, when increasing the total alloying addition.

From Fig. 4, it could be seen that the increasing Nd/Gd ratio would much promote the quantity of fiber-like crushed second phase when keeping the alloying addition the same. This fiber-like second phase consists of a quantity of polygonal phase, which deteriorates the plasticity of the alloy badly. However, the particle-like second phase would not concentrate the stress rapidly, which is not so bad to the plasticity. It could also be seen that the increasing alloying addition also promotes the mechanical properties and deteriorates the plasticity.

The alloys have almost the same strength in spite of owning different Nd/Gd ratios. It requires further discussion. There are three kinds of strengthening mechanisms in Mg–RE alloys: solid solution strengthening, refined crystalline strengthening and precipitated-phase strengthening [21,22]. When rare earth element is solved in Mg, atomic radius distinction between RE and Mg brings in a stress field, called solid solution strengthening. The remarkable precipitation strengthening is attributable to precipitate phases formed on prismatic planes of α-Mg matrix phase, providing the most effective obstacles to basal dislocation slip [23]. In this work, solid solution strengthening and precipitated-phase strengthening should be the main function. According to the small solid solubility of Nd in Mg, Nd is more inclined to segregate at the grain boundaries. Thus, the quantity of fiber-like second phase was much increased by the rising Nd/Gd ratios, as shown in Fig. 4. Meantime, the solid solution strengthening effect will decrease correspondingly. The same mechanical properties should be attributed to the same accumulated effects of solid solution and precipitation strengthening effects.

The mechanical properties are obviously promoted after T5 treatment. From Table 2, it can be seen that UTS of Alloy 2 enlarges from 340 MPa to 379 MPa, and TYS increases from 300 MPa to 332 MPa, while UTS and TYS of Alloy 4 increase just by 27 MPa and 17 MPa, respectively. Likewise, the situation is similar to the comparison between Alloy 1 and Alloy 3. Therefore, it indicates that the smaller the Nd/Gd value is, the larger the promotion is. Diverse aging hardening responses could be attributed to the different aging hardness behaviors of Gd and Nd. The hardness increase of Mg–Nd alloys is observed beginning with the lowest aging time of 0.75 h and continues
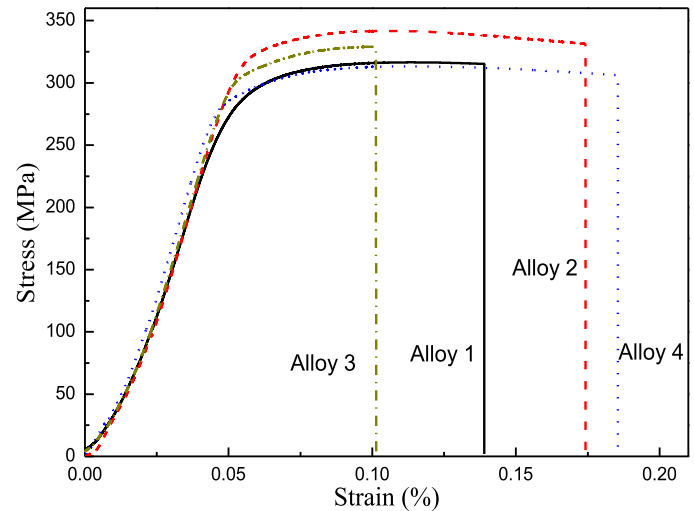

Fig. 6. Stress strain curves of the alloys at 200 °C.

gradually up to the maximum, while hardness increase of Mg–Gd alloys ascends deeply after a stage increasing slowly [24]. Thus, the aging strengthening effect proves to be outstanding at a small Nd/Gd value. On the other hand, it always requires a supersaturated matrix to obtain outstanding hardening response. However, larger Nd/Gd ratio indicates less amount of RE solved in the matrix. The alloy with larger Nd/Gd ratio receives a weaker aging response.

Fig. 6 shows the stress strain curves of the peak-aging extruded alloys at 200 °C. Compared to the room temperature, the stress of the peak-aging alloys at 200 °C is a bit lower and the elongations get much promoted. The peak-aged extruded Mg-Alloy 2 (10Gd–3Y–4Nd–0.6Zr) exhibits the highest ultimate tensile stress and tensile yielding stress at the elevated temperature of 200 °C, which are 342 MPa and 260 MPa, respectively. The performance of mechanical properties at elevated temperature should be ascribed to the dispersed precipitations, while promotion of the elongation benefits from the motivation of slip systems at 200 °C.

4. Conclusion

The investigated as-cast Mg–Gd–Y–Nd–Zr alloys mainly consist of α-Mg and β-Mg$_5$(GdYNd). Precipitations spread along the grain boundaries discontinuously, as a state of pseudo-eutectic. Precipitations in the as-cast alloys tend to increase as the Nd/Gd value rises up. With the Nd/Gd value increasing, the fiber-like second phase increases rapidly, and the tiny particle-like phase is

decreased. By enlarging Nd/Gd value, mechanical properties of the extruded alloys will not decrease. The aging hardening response of the investigated alloy also decreases with the increasing Nd/Gd ratios. The peak-age extruded alloy Mg–10Gd–3Y–4Nd–0.6Zr (wt.%) exhibits the highest ultimate tensile stress and tensile yielding stress at room temperature and the elevated temperature of 200 °C, which are 379 MPa and 332 MPa at room temperature, and 342 MPa and 260 MPa at 200 °C, respectively.

Acknowledgements

Reference

[1] B. Smola, I. Stulıková, F. von Buch, B.L. Mordike, Mater. Sci. Eng, A 324 (2002) 113–117.
[2] C.J. Bettles, M.A. Gibson, Adv. Eng. Mater. 5 (2003) 859–865.
[3] H.L. Chen, L. Lin, P.L. Mao, Z. Liu, J. Magnes. Alloy. 3 (2015) 197–202.
[4] J. Li, R. Chen, Y. Ma, W. Ke, J. Magnes. Alloy. 1 (2013) 346–351.
[5] X. Liu, Q. Le, Z. Zhang, L. Bao, Z. Fan, J. Cui, J. Magnes. Alloy. 2 (2014) 342–348.
[6] V. Janik, D.D. Yin, Q.D. Wang, S.M. He, C.J. Chen, Z. Chen, et al., Mater. Sci. Eng, A 528 (2011) 3105–3112.
[7] Q. Peng, J. Wang, Y. Wu, L. Wang, Mater. Sci. Eng, A 433 (2006) 133–138.
[8] X. Hou, Q. Peng, Z. Cao, S. Xu, S. Kamado, L. Wang, et al., Mater. Sci. Eng, A 520 (2009) 162–167.
[9] M.E. Drits, Z.A. Sviderskaya, L.L. Rokhlin, N.I. Nikitina, Met. Sci. Heat Treat. 21 (1979) 887–889.
[10] I.A. Anyanwu, S. Kamado, Y. Kojima, Mater. Trans. 42 (2001) 1212–1218.
[11] X.B. Liu, R.S. Chen, E.H. Han, J. Alloys Compd. 465 (2008) 232–238.
[12] R. Wang, J. Dong, L. Fan, P. Zhang, W. Ding, Trans. Nonferrous. Met. Soc. China 18 (Suppl. 1) (2008) s189–s193.
[13] S.M. He, X.Q. Zeng, L.M. Peng, X. Gao, J.F. Nie, W.J. Ding, J. Alloys Compd. 427 (2007) 316–323.
[14] Y. Gao, Q. Wang, J. Gu, Y. Zhao, Y. Tong, J. Kaneda, J. Rare Earth 26 (2008) 298–302.
[15] X. Zhang, L. Meng, C. Fang, P. Peng, F. Ja, H. Hao, Mater. Sci. Eng, A 586 (2013) 19–24.
[16] N. Liakishev, Phase Diagrams of Binary Metal Systems, Mechanical Engineering, Moscow, 1996.
[17] X. Liu, Q. Le, Z. Zhang, L. Bao, J. Cui, Indian J. Eng. Mater. Sci. 22 (2015) 14–22.
[18] L. Wang, C. Xing, X. Hou, Y. Wu, J. Sun, L. Wang, Mater. Sci. Eng, A 527 (2010) 1891–1895.
[19] Q.M. Peng, Y.M. Wu, D.Q. Fang, J. Meng, L.M. Wang, J. Alloys Compd. 430 (2007) 252–256.
[20] Q. Peng, X. Hou, L. Wang, Y. Wu, Z. Cao, L. Wang, Mater. Des. 30 (2009) 292–296.
[21] M. Yoo, Metall. Trans. A 12 (1981) 409–418.
[22] G. Nussbaum, P. Sainfort, G. Regazzoni, H. Gjestland, Scr. Metall. 23 (1989) 1079–1084.
[23] J. Nie, Scr. Mater. 48 (2003) 1009–1015.
[24] L.L. Rokhlin, Magnesium Alloys Containing Rare Earth Metals: Structure and Properties, Taylor & Francis, London, 2003.